AAAS
Ultrafast Science
Volume 2022, Article ID 9812478, 8 pages
https://doi.org/10.34133/2022/9812478

Ultrafast Science
A SCIENCE PARTNER JOURNAL

Research Article

Generating Isolated Attosecond X-Ray Pulses by Wavefront Control in a Seeded Free-Electron Laser

Yaozong Xiao,[1,2] **Chao Feng**,[1,2,3] **and Bo Liu**[1,2,3]

[1]*Shanghai Institute of Applied Physics, Chinese Academy of Sciences, Shanghai 201800, China*
[2]*University of Chinese Academy of Sciences, Beijing 100049, China*
[3]*Shanghai Advanced Research Institute, Chinese Academy of Sciences, Shanghai 201210, China*

Correspondence should be addressed to Chao Feng; fengchao@zjlab.org.cn

Received 1 April 2022; Accepted 6 July 2022; Published 30 July 2022

We proposed a simple method based on the seeded free-electron laser (FEL) to generate fully coherent X-ray pulses with durations at dozens of attosecond level. The echo-enabled harmonic generation technique is utilized to generate the fully coherent laser pulse covering the water-window range. A wavefront rotation laser is adopted as the seed to tailor the longitudinal contour of the radiation pulse. Due to the sensitivity of seeded FEL to external lasers, this method can effectively inhibit the bunching of the adjacent regions while preserving an isolated bunching in the middle. Sending such an electron beam into a short undulator, simulation results show that ultrashort X-ray pulses with peak power of GW level and pulse duration as short as 86 attoseconds can be generated. The proposed scheme can make it possible to study the electronic dynamic of the valence electrons of which the time scale is about 100 attoseconds and may open up a new frontier of ultrafast science.

1. Introduction

The pump-probe technique is usually an effective means to study ultrafast time-varying phenomena, in which a pump laser is applied to initiate the sample and then another delayed pulse is applied to probe into it [1–5]. The temporal resolution of this technique directly depends on the pulse length of the pump and probe lasers. The shorter the pulse length, the higher the temporal resolution can be achieved. The ultrashort pulses of attosecond magnitude can even be used to study the dynamics of electrons, opening up plenty of new fields of ultrafast science, such as ultrahigh resolution imaging, attosecond electron dynamics, and the transformation process of material structure in the biological systems [6–9].

Recently, ultrafast science has made great advances. In the extreme ultraviolet wavelength, the pulse duration has been pushed to the order of tens of attoseconds based on high harmonic generation (HHG) [10–13]. The principle of HHG is to utilize the infrared (IR) intense laser field to drive electrons in the atomic or molecular gas, resulting in the high-order harmonic conversion of driving laser fields. Studies of the motion of electrons near atomic nucleus require attosecond X-ray pulses; however, the conversion efficiency of HHG would decrease dramatically in the soft X-ray range.

The urgent need of intense X-ray attosecond pulses, especially in the water-window range, has promoted the development of attosecond X-ray free-electron lasers (FELs) [14–21]. Several schemes have been proposed to shorten the pulse duration of FEL. For example, by using a low-charge electron beam, it is possible to significantly shorten the bunch length and then shorten the final radiation pulse duration [22, 23]. Alternatively, a slotted foil can be placed in the center of the bunch compressor to selectively destroy the emittance of electron beam so as to make only a small fraction of it to lase [24, 25]. But in soft X-ray range, both of the above methods can only generate pulses of a few femtoseconds. A common method for producing ultrafast pulses is the enhanced self-amplified spontaneous emission (ESASE) technique, which utilizes few-cycle lasers [26] or self-modulation [27] to manipulate the longitudinal distribution of electron beams and then to enhance the local peak current for generating pulses of hundreds of attoseconds. In addition, there are many improvements based on the ESASE

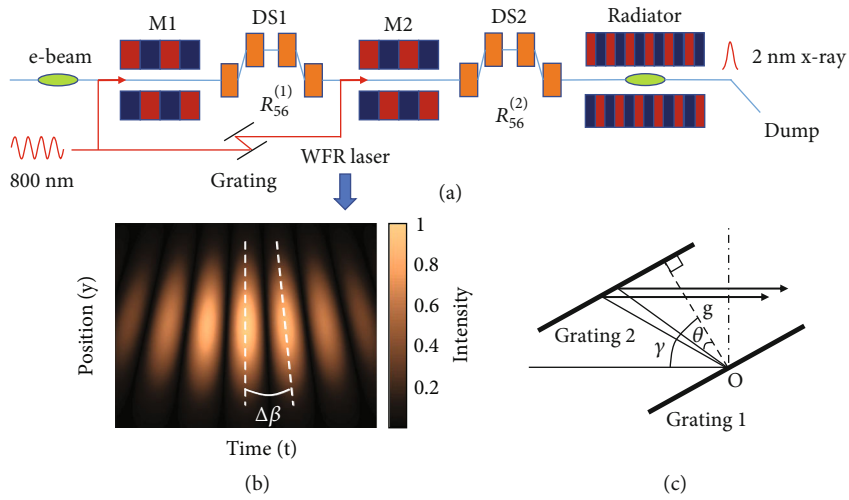

Figure 1: Schematic of our scheme. The layout for attosecond X-ray pulse generation (a) by using a wavefront rotation laser (b) generated through a double-grating configuration (c).

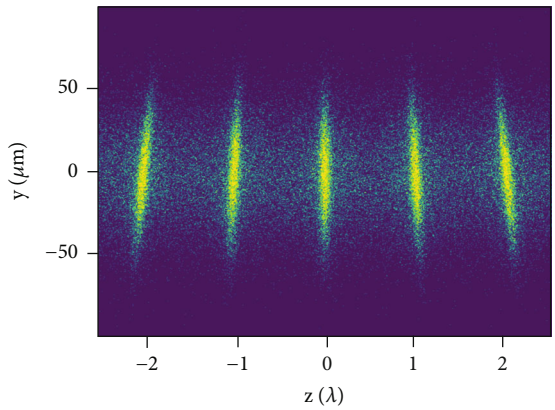

Figure 2: The electron beam distribution in the y-z plane after energy and density modulation process with a WFR laser.

to enhance the peak power or reduce the duration of radiation pulse [19, 20, 28–30], whereas it is still very challenging to generate stable and isolated X-ray pulses with durations of dozens of attoseconds since SASE originates from the shot noise of electron beams and the shortest pulse duration is eventually limited by the slippage effect. To overcome these problems, several methods based on seeded FELs have been proposed [31, 32]. However, in these methods, few-cycle ultrashort laser pulses are generally required, leading to additional challenges for the laser generation and transmission.

In this paper, we propose a simple and feasible method based on the echo-enabled harmonic generation (EEHG) [33–36] to generate intense isolated X-ray pulses covering the water-window range with a duration of tens of attoseconds. A wavefront rotation (WFR) laser is employed to control the distribution of the microbunching and make sure only a small part of electrons can lase. The generated isolate attosecond pulses are natural synchronization to external lasers, making them capable of driving high resolution pump-probe experiments and providing a new avenue for attosecond sciences.

2. Methods

The schematic of our proposed scheme is shown in Figure 1(a), which is similar to the conventional EEHG setup with two modulators, two dispersion segments, and a radiator. And the difference is that the second seed laser is sent through a dispersion element, e.g., double gratings, to induce spatiotemporally coupling and control the wavefront of the beam. The rotation angle of the wavefront at any position can be given by $\beta = \omega(y)/\omega_0$, where $\omega(y)$ is the angular frequency of the laser field at position y and ω_0 is the central angular frequency of the laser field. The wavefronts rotate with a velocity $v_r = \partial\beta/\partial y = [\partial\omega(y)/\partial y]/\omega_0$, and then, the angle between adjacent wavefronts is $\Delta\beta = v_r T$, where T is the interval between the wavefronts.

A diagram of the wavefront rotation lasers is shown in Figure 1(b). It can be intuitively understood that the wavelength of the laser is different at different transverse positions; as a result, the wavefront is rotated. A tunable WFR can be obtained by changing the dispersion induced by two parallel gratings. As shown in Figure 1(c), for grating 1, let the incident and diffraction angle be γ and θ, respectively; then, the relationship between them follows the grating equation $\sin\theta + \sin\gamma = n\lambda/b$, where n is the diffraction order and b is the grating constant. According to the geometric relationship, the optical path P and the displacement Δy in the transverse direction after the double gratings can be obtained:

$$P = \frac{g}{\cos\theta} \cdot [1 + \cos(\gamma - \theta)],$$
$$\Delta y = g\cos\gamma \cdot (\tan\theta_0 - \tan\theta), \quad (1)$$

where g is the vertical interval between two gratings and θ_0 is the diffraction angle of the central wavelength after passing through the first grating.

The rotation of the seed laser wavefront will result in a rotation of the microbunching. Simulations have been performed for a simple energy and density modulation process

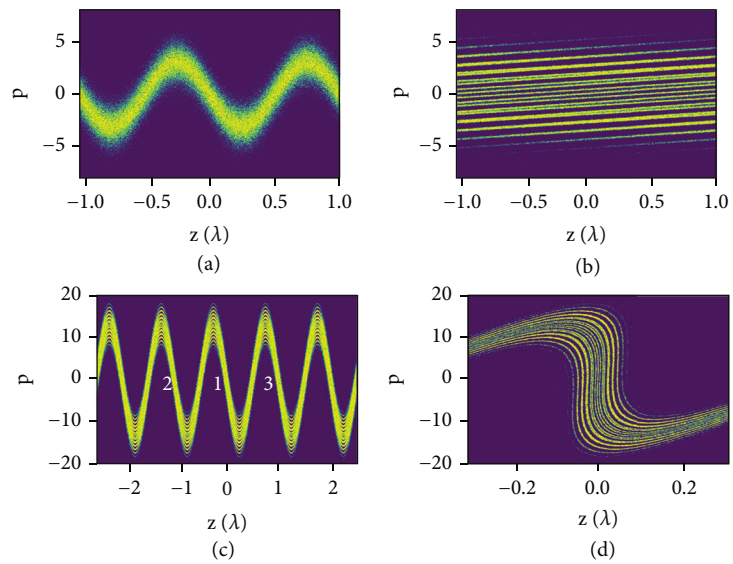

Figure 3: Longitudinal phase space evolution. Schematic of the phase space of electron beams in our proposed scheme: after (a) the first modulator, (b) the first dispersion segment, (c) the second modulator, and (d) the second dispersion segment.

Table 1: Main parameters of the proposed scheme.

Parameters	Value	Unit
Electron beam energy	2.5	GeV
Peak current	3	kA
Normalized emittance	0.43	mm·mrad
Energy spread (rms)	350	keV
Modulator period in M1 and M2	15	cm
Modulator period numbers in M1/M2	6/1	—
Radiator period	3	cm
Radiator period numbers	20	—

with a WFR laser and a single-period modulator. The simulation result is shown in Figure 2, where one can find that that the spatial characteristics of the WFR laser wavefront are coupled to the distribution of the electron beam.

To illustrate the basic process of generating attosecond pulses with the proposed method, let us focus on the evolution of longitudinal phase space of EEHG. Despite its simplicity, it contains the key dynamic processes of modulation and microbunching generation. In the proposed scheme, an 800 nm laser is first applied as a seed to interact with the relativistic electron beam in the first modulator (M1) to introduce an energy modulation whose dimensionless amplitude is $A_1 = \Delta E_1/\sigma_E$, where σ_E is the rms energy spread. The basic principles are similar to EEHG in Ref. [34]. After passing through M1, the energy modulation is completed, and the phase space evolves into Figure 3(a). The electron beam then passes through the first dispersion segment (DS1) with large dispersion intensity, and after that, the energy modulation formed in M1 is washed away, and fine energy band structures are introduced simultaneously in the longitudinal phase space as shown in Figure 3(b). Here, the normalized dispersion intensity is $B_1 = kR_{56}^{(1)}\sigma_E/E_0$, where k is the wave number of seed lasers and E_0 is the average beam energy. Subsequently, an 800 nm laser with rotating wavefront is employed to ulteriorly modulate the electron beam in the second modulator (M2) to introduce a large energy modulation $A_2 = \Delta E_2/\sigma_E$. After passing through the second magnetic chicane (DS2), whose normalized dispersion intensity is $B_2 = kR_{56}^{(2)}\sigma_E/E_0$, the middle portion of the longitudinal phase space (region 1) in Figure 3(c) will convert to the structures in Figure 3(d). Since the fine structure of EEHG is quite sensitive to the wavefront tilt of seed lasers, the output pulse duration can be tuned and controlled by changing the wavefront of seed laser pulses. When the WFR is large enough, isolated radiation pulses can be generated in the following radiator.

Note that the microbunching of EEHG is very sensitive to the wavefront of the seed laser. Due to the inherent nature of the WFR lasers, the wavefronts on both sides will be tilted. This degrades the high harmonic bunching on the adjacent regions (like regions 2 and 3) after passing through DS2.

3. Simulations for the Generation of Isolated Attosecond Pulses

To illustrate the possible performance of the proposed method, in this section, we will perform three-dimensional simulations with realistic parameters from the SwissFEL [37] as listed in Table 1. The seed lasers we employed are 800 nm IR lasers with initial pulse durations of 100 fs. The simulation of FEL gain processes is conducted by *GENESIS* [38].

As shown in Figure 4, after passing through two parallel gratings with a vertical dispersion, spatiotemporally coupling has been induced in the seed laser. The variation of pulse length in the longitudinal direction is very small (from 100 fs to about 100.3 fs) and can be basically ignored. Moreover, we define $\Delta\lambda$ (here, $\Delta\lambda = 3$ nm) as the maximum

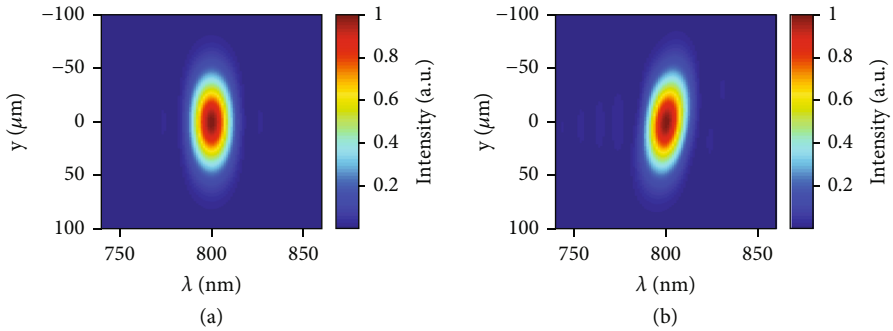

Figure 4: Frequency distribution in the y direction (a) before and (b) after the double grating.

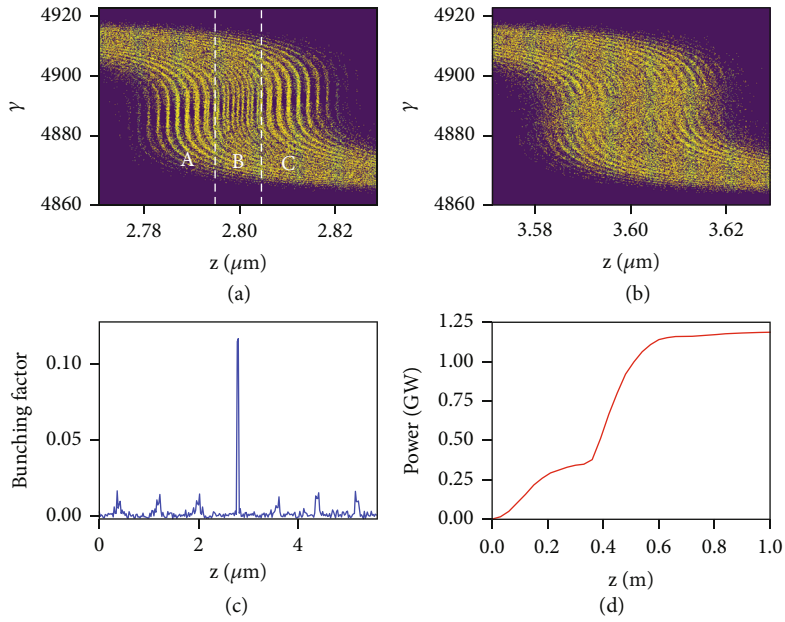

Figure 5: Performance of the proposed technique. Phase space of the electron beam in region 1 (a) and region 3 (b) at the exit of DS2. (c) Bunching factor distribution of the electron beam. (d) The gain curve for the ultrashort pulse in the radiator.

wavelength difference of the WFR laser in the y direction of the electron beam, which represents the transverse dispersion strength. The larger $\Delta\lambda$ is, the stronger the dispersion the laser is subjected to. As a result, the wavefront of the seed laser is rotated with an angular difference of $\Delta\beta \approx 60\,\mu$rad between adjacent cycles. This laser pulse has been adopted as the second seed laser of EEHG.

The energy modulation amplitudes for EEHG have been chosen to be $A_1 = 3, A_2 = 30$, corresponding to laser powers of 250 MW and 150 GW, respectively. The optimized value of normalized dispersion for 400th harmonic is $B_1 \approx 13.03$, $B_2 \approx 0.0339$. With these parameters, the electron beams pass through the modulator and dispersion sections. Except the central slice where the wavefront is maintained, most of the fine structures of EEHG have been washed out. Figures 5(a) and 5(b) compare the longitudinal phase space at region 1 and region 3 in Figure 3, and the results show that only the central part of the beam produces significant bunching as shown in Figure 5(c). For regions 2 and 3, the fine structures are mixed together due to the transverse tilt of the microbunching. At the exit of DS2, the bunching factor in region 1 for the 400th harmonic (2 nm X-ray for an 800 nm seed laser) is about 0.12, and that for other positions is just a few times higher than the shot noise level of about 1×10^{-3}.

The bunching region in Figure 5(a) can be divided into three parts, namely, parts A, B, and C. The bunching factor in the middle part (B) of the main peak is significantly smaller than those in both sides (A and C). The large bunching factor will initiate coherent radiation at the very beginning of the radiator, as shown in Figure 5(d); the power grows proportional to the square of the undulator length in the first 0.2 m. After that, the radiation from part A slips to part B, and the radiation from part C starts to slip out of the bunching region. As a result, the power growth becomes relative slow until 0.4 m. Rapid power gain will be recovered after 0.4 m when the radiation from part A slips

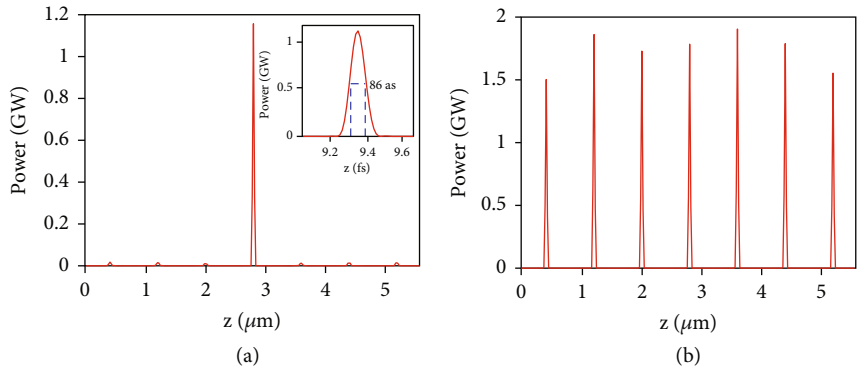

FIGURE 6: Comparison of the performances for different setups. Radiation pulses from the proposed technique with a WFR laser (a) or a conventional laser (b) as the second seed.

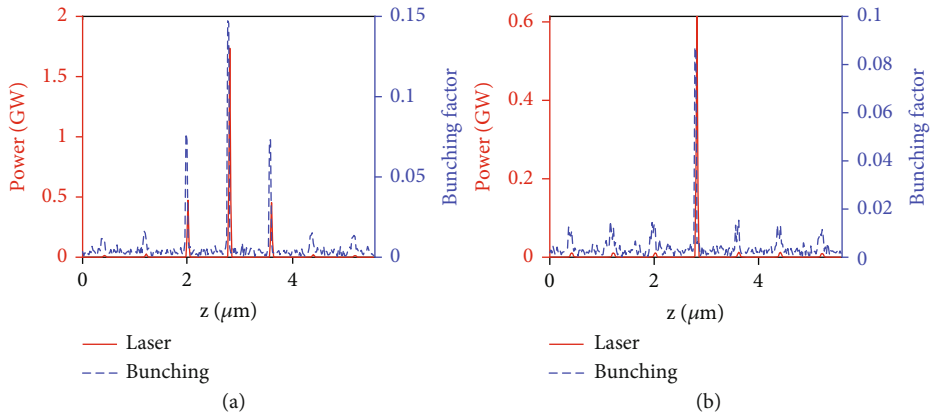

FIGURE 7: Results for different WFR angles. Radiation pulses (red solid line) and bunching factor distributions (blue dashed line) with $\Delta\lambda = 1$ nm (a) and $\Delta\lambda = 5$ nm (b).

to part C. After 0.6 m, the initial radiation pulse slips out of the bunching region, and the power growth is terminated.

The output pulse duration is determined by both the bunching distribution and the slippage effect; however, the fast gain in the short undulator makes the pulse duration shorter than the slippage length. The radiation pulse at 0.6 m of the radiator is shown in Figure 6(a), where one can find an isolated attosecond pulse with peak of 1.15 GW and pulse duration of 86 as (FWHM) has been generated. The energy of the entire radiation pulse is about 0.113 μJ, and the signal-to-noise ratio is about 87.2%. For comparison purpose, we also performed simulations for a normal EEHG with the same parameters. The results are given in Figure 6(b), where an attosecond pulse train has been generated. Compared with conventional laser case, the maximal bunching factor in the proposed method decreases a little on account of the energy modulation amplitude variation in the transverse direction. As a result, the peak power decreases from 1.8 GW to 1.15 GW.

Figure 7illustrates the influence of different WFR angles on FEL radiation profiles. With a smaller WFR angle of $\Delta\beta \approx 20\,\mu$rad, corresponding to $\Delta\lambda = 1$ nm, the bunching factor and the peak power of the main peak, which are 0.147 and 1.74 GW, respectively (decreasing slightly compared with conventional laser case), are higher than the case with $\Delta\lambda = 3$ nm. However, the smaller tilt angle also leads to significant satellite pulses, as shown in Figure 7(a). With a larger WFR angle of $\Delta\beta \approx 100\,\mu$rad, corresponding to $\Delta\lambda = 5$ nm, the satellite pulses can be sufficiently suppressed, while the peak power of the main pulse also decrease, as shown in Figure 7(b). The optimized $\Delta\lambda$ in this simulation is about 3 nm.

In the proposed method, the laser pointing instability and electron beam orbit variation would affect the FEL performance. Multishot simulations have been performed with random jitters (10% of the transverse sizes of the electron beam and the seed laser) of both the electron beam orbit and the laser pointing. Simulation results are summarized in Figure 8. The average power is calculated to be about 1.04 GW with a relative jitter of 3.7% (rms). Figure 8(b) also shows the fluctuation of the output pulse duration where the average value is 85.4 attoseconds with a standard deviation of 1.3 attoseconds.

It has been reported in Ref. [31] that isolated ultrashort pulses can also be generated by utilizing a few-cycle laser as the second seed in EEHG. For comparison, we performed simulations for this scenario with the same parameters given above, i.e., $A_1 = 3$, $A_2 = 30$, $B_1 \approx 13.03$, $B_2 \approx 0.0339$, and $h = 400$. A few-cycle laser with a pulse duration of 15 femtoseconds (FWHM) was adopted as the second seed laser of EEHG. After passing through the modulation and

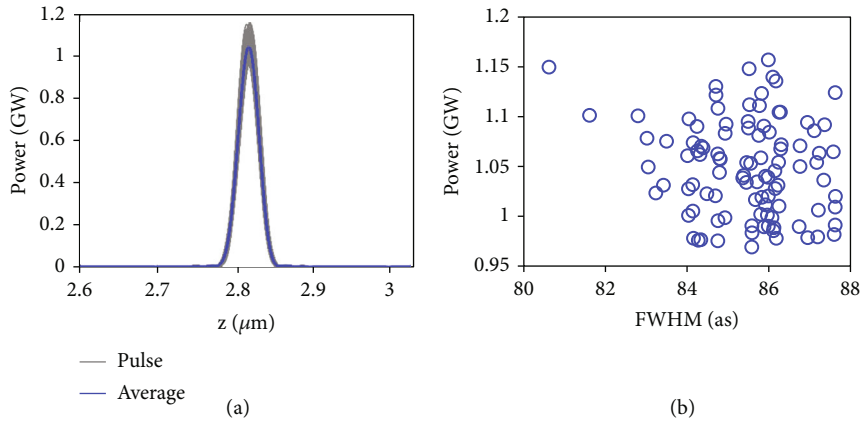

Figure 8: Multishot simulations for the proposed method. (a) The gray curves are the results of multishot (100 shots) simulations, and the blue curve is the average of these results. (b) Peak powers of output pulses and their corresponding pulse durations.

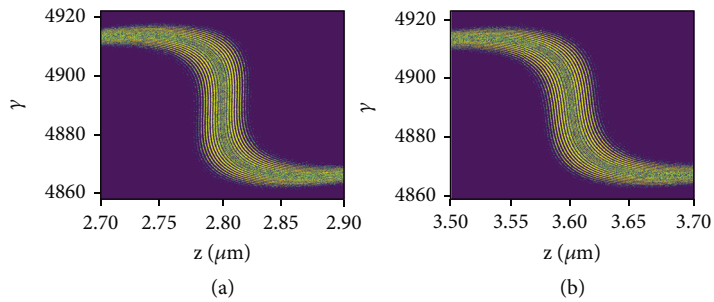

Figure 9: Longitudinal phase spaces of an electron beam at different locations of the seed laser (15 fs few-cycle lasers) in the central cycle (a) and the nearest side cycle (b).

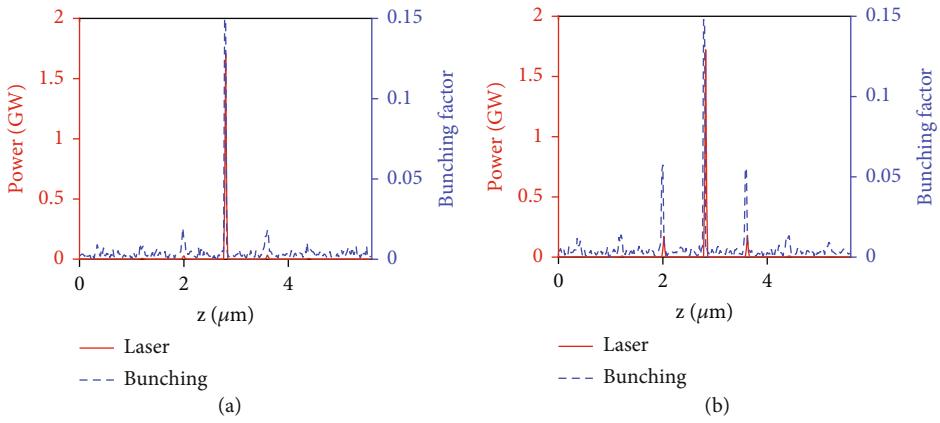

Figure 10: Results for different pulse durations. Bunching factor distributions after DS2 (blue dashed line) and the corresponding radiation pulses (red solid line) when the second seed laser of EEHG is replaced by the few-cycle laser with pulse duration of 15 fs (a) and 18 fs (b).

dispersion sections, the longitudinal phase spaces at different locations of the seed laser are shown in Figure 9. It can be seen that, compared with Figure 9(a), beamlets in Figure 9(b) are obviously not effectively compressed. As a result, only the electron beam in the central cycle produces significant bunching, as shown in Figure 10(a). Sending such an electron beam into a radiator, isolated radiation pulse with the pulse duration of 86 attoseconds and peak power of 1.7 GW can be generated.

To generate isolated radiation pulse, the duration of few-cycle lasers should be short enough. As shown in Figure 10(b), when the duration of laser pulse is increased to 18 fs, the bunching factors at nearest side peaks cannot be sufficiently suppressed, resulting in side peaks with power

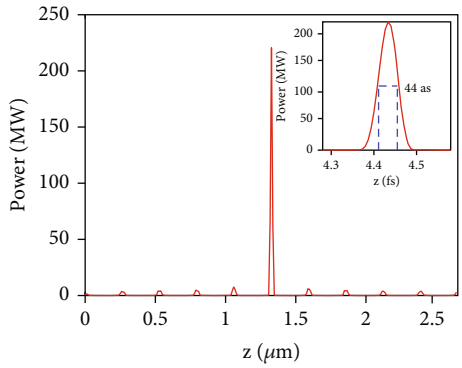

FIGURE 11: Radiation pulse when the wavelength of seed laser is 266 nm.

of about 175 MW. Therefore, it puts forward strict requirements on both the pulse duration and carrier phase of the few-cycle laser.

In addition, the duration of the radiation pulse from the proposed technique can be further reduced by adopting seed lasers in UV range, where the few-cycle lasers are hardly to obtain. We simulated the case that the seed laser wavelength is 266 nm, and the parameters we adopted are $A_1 = 3$, $A_2 = 20$, $B_1 \approx 6.37$, $B_2 \approx 0.0519$, $h = 133$, and $\Delta\lambda = 2.5\,\text{nm}$ $(\Delta\beta \approx 50\,\mu\text{rad})$. The final radiation pulse length is about 44 attoseconds, which is reduced by nearly twice, and the peak power is about 220 MW as shown in Figure 11. To suppress the side peaks, a shorter laser pulse with initial duration of 18 fs is required. Because it is necessary to ensure the energy modulation intensity of different wavelength components in M2, the pulse length of the second seed laser should be short enough.

4. Conclusion

In conclusion, we propose a feasible method that holds the capability of generating isolated attosecond X-ray pulses covering the water-window range based on the EEHG technique. The second seed laser of EEHG is replaced by a wavefront rotation laser, so as to inhibit the formation of side peaks. We show that isolated X-ray coherent pulses with output wavelength as short as 2 nm, peak power of 1.15 GW, and duration of 86 attoseconds can be generated. In our scheme, what we used is a 100 fs conventional laser, and carrier-envelope phase-lock of the seed laser is not necessary for stabilizing the FEL power. This greatly relaxes the requirement for the seed laser system. However, a carrier-envelope phase-locked seed laser would reduce the timing jitter of the FEL output. Moreover, the duration of the output pulses can be further reduced to 44 attoseconds by using a wavefront rotation laser at shorter wavelength. This kind of coherent X-ray light sources is particularly valuable for the field of ultrafast science, such as the study of electronic dynamics of the valence electrons whose time scale is about 100 attoseconds.

Data Availability

The corresponding author can provide relevant data if the demand is reasonable.

Conflicts of Interest

The authors declare that there is no conflict of interest in the publishing this article.

Authors' Contributions

Chao Feng conceived the idea and scheme. Chao Feng and Bo Liu supervised the project. Yaozong Xiao performed the simulations and analyzed the results. Contribution of all authors to the writing of the manuscript is equal.

Acknowledgments

The authors thank H. Sun, W. J. Fan, and X. F. Wang for helpful discussions and useful comments. This work was supported by the National Natural Science Foundation of China (12122514, 11975300) and the Shanghai Science and Technology Committee Rising-Star Program (20QA1410100).

References

[1] F. Krausz and M. Ivanov, "Attosecond physics," *Reviews of Modern Physics*, vol. 81, no. 1, pp. 163–234, 2009.

[2] E. Allaria, F. Bencivenga, R. Borghes et al., "Two-colour pump-probe experiments with a twin-pulse-seed extreme ultraviolet free-electron laser," *Nature Communications*, vol. 4, no. 1, article BFncomms3476, pp. 2476-2477, 2013.

[3] H. Mashiko, T. Yamaguchi, K. Oguri, A. Suda, and H. Gotoh, "Characterizing inner-shell with spectral phase interferometry for direct electric-field reconstruction," *Nature Communications*, vol. 5, no. 1, article BFncomms6599, 2014.

[4] E. Ferrari, C. Spezzani, F. Fortuna et al., "Widely tunable two-colour seeded free-electron laser source for resonant- pump resonant-probe magnetic scattering," *Communications*, vol. 7, no. 1, article 10343, pp. 1–8, 2016.

[5] A. Picón, C. S. Lehmann, C. Bostedt et al., "Hetero-site-specific X-ray pump-probe spectroscopy for femtosecond intramolecular dynamics," *Nature Communications*, vol. 7, no. 1, article BFncomms11652, pp. 1–6, 2016.

[6] M. F. Kling and M. J. J. Vrakking, "Attosecond electron dynamics," *Annual Review of Physical Chemistry*, vol. 59, no. 1, pp. 463–492, 2008.

[7] S. Li, T. Driver, P. Rosenberger et al., "Attosecond coherent electron motion in Auger-Meitner decay," *Science*, vol. 375, no. 6578, pp. 285–290, 2022.

[8] A. Rudenko, L. Inhester, K. Hanasaki et al., "Femtosecond response of polyatomic molecules to ultra-intense hard X-rays," *Nature*, vol. 546, no. 7656, article BFnature22373, pp. 129–132, 2017.

[9] I. Schlichting and J. Miao, "Emerging opportunities in structural biology with X-ray free-electron lasers," *Current Opinion in Structural Biology*, vol. 22, no. 5, article S0959440X12001261, pp. 613–626, 2012.

[10] E. Goulielmakis, M. Schultze, M. Hofstetter et al., "Single-cycle nonlinear optics," *Science*, vol. 320, no. 5883, pp. 1614–1617, 2008.

[11] J. Li, J. Lu, A. Chew et al., "Attosecond science based on high harmonic generation from gases and solids," *Nature Communications*, vol. 11, no. 2748, article 16480, pp. 1–13, 2020.

[12] M. Hentschel, R. Kienberger, C. Spielmann et al., "Attosecond metrology," *Nature*, vol. 414, no. 6863, article BF35107000, pp. 509–513, 2001.

[13] H. Vincenti and F. Quéré, "Attosecond lighthouses: how to use spatiotemporally coupled light fields to generate isolated attosecond pulses," *Physical Review Letters*, vol. 108, no. 11, article 113904, 2012.

[14] L. R. Elias, W. M. Fairbank, J. M. J. Madey, H. A. Schwettman, and T. I. Smith, "Observation of stimulated emission of radiation by relativistic electrons in a spatially periodic transverse magnetic field," *Physical Review Letters*, vol. 36, no. 13, pp. 717–720, 1976.

[15] D. A. G. Deacon, L. R. Elias, J. M. J. Madey, G. J. Ramian, H. A. Schwettman, and T. I. Smith, "First operation of a free-electron laser," *Physical Review Letters*, vol. 38, no. 16, pp. 892–894, 1977.

[16] P. Emma, R. Akre, J. Arthur et al., "First lasing and operation of an angstrom-wavelength free-electron laser," *Nature Photonics*, vol. 4, no. 9, article BFnphoton2010176, pp. 641–647, 2010.

[17] T. Ishikawa, H. Aoyagi, T. Asaka et al., "A compact X-ray free-electron laser emitting in the sub-angstrom region," *Nature Photonics*, vol. 6, no. 8, article BFnphoton2012141, pp. 540–544, 2012.

[18] E. Allaria, D. Castronovo, P. Cinquegrana et al., "Two-stage seeded soft-X-ray free-electron laser," *Nature Photonics*, vol. 7, no. 11, article BFnphoton2013277, pp. 913–918, 2013.

[19] Z. Wang, C. Feng, and Z. Zhao, "Generating isolated terawatt-attosecond x-ray pulses via a chirped-laser-enhanced high-gain free-electron laser," *Physical Review Accelerators and Beams*, vol. 20, no. 4, article 040701, 2017.

[20] Z. Qi, C. Feng, H. Deng, B. Liu, and Z. Zhao, "Generating attosecond X-ray pulses through an angular dispersion enhanced self-amplified spontaneous emission free electron laser," *Physical Review Accelerators and Beams*, vol. 21, no. 12, article 120703, 2018.

[21] C. Feng, J. Chen, and Z. Zhao, "Generating stable attosecond x-ray pulse trains with a mode-locked seeded free-electron laser," *Physical Review Special Topics-Accelerators and Beams*, vol. 15, no. 8, article 080703, 2012.

[22] S. Reiche, P. Musumeci, C. Pellegrini, and J. B. Rosenzweig, "Development of ultra-short pulse, single coherent spike for SASE X-ray FELs," *Nuclear Instruments and Methods in Physics Research Section A: Accelerators, Spectrometers, Detectors and Associated Equipment*, vol. 593, no. 1-2, article S0168900208006207, pp. 45–48, 2008.

[23] Y. Ding, A. Brachmann, F. J. Decker et al., "Measurements and simulations of ultralow emittance and ultrashort electron beams in the Linac coherent light source," *Physical Review Letters*, vol. 102, no. 25, article 254801, 2009.

[24] P. Emma, K. Bane, M. Cornacchia et al., "Femtosecond and subfemtosecond X-ray pulses from a self-amplified spontaneous-emission–based free-electron laser," *Physical Review Letters*, vol. 92, no. 7, article 074801, 2004.

[25] Y. Ding, C. Behrens, R. Coffee et al., "Generating femtosecond X-ray pulses using an emittance-spoiling foil in free-electron lasers," *Applied Physics Letters*, vol. 107, no. 19, article 191104, 2015.

[26] A. A. Zholents, "Method of an enhanced self-amplified spontaneous emission for x-ray free electron lasers," *Physical Review Special Topics-Accelerators and Beams*, vol. 8, no. 4, article 040701, 2005.

[27] J. Duris, S. Li, T. Driver et al., "Tunable isolated attosecond X-ray pulses with gigawatt peak power from a free-electron laser," *Nature Photonics*, vol. 14, no. 1, article 549, pp. 30–36, 2020.

[28] Y. Ding, Z. Huang, D. Ratner, P. Bucksbaum, and H. Merdji, "Generation of attosecond x-ray pulses with a multicycle two-color enhanced self-amplified spontaneous emission scheme," *Physical Review Special Topics-Accelerators and Beams*, vol. 12, no. 6, article 060703, 2009.

[29] Z. Zhang, J. Duris, J. P. MacArthur, Z. Huang, and A. Marinelli, "Double chirp-taper x-ray free-electron laser for attosecond pump-probe experiments," *Physical Review Accelerators and Beams*, vol. 22, no. 5, article 050701, 2019.

[30] J. Duris, Z. Zhang, J. MacArthur, Z. Huang, and A. Marinelli, "Superradiant amplification in a chirped-tapered x-ray free-electron laser," *Physical Review Accelerators and Beams*, vol. 23, no. 2, article 020702, 2020.

[31] D. Xiang, Z. Huang, and G. Stupakov, "Generation of intense attosecond x-ray pulses using ultraviolet laser induced microbunching in electron beams," *Physical Review Special Topics-Accelerators and Beams*, vol. 12, no. 6, article 060701, 2009.

[32] T. Tanaka, "Proposal to generate an isolated monocycle x-ray pulse by counteracting the slippage effect in free-electron lasers," *Physical Review Letters*, vol. 114, no. 4, article 044801, 2015.

[33] G. Stupakov, "Using the beam-echo effect for generation of short-wavelength radiation," *Physical Review Letters*, vol. 102, no. 7, article 074801, 2009.

[34] D. Xiang and G. Stupakov, "Echo-enabled harmonic generation free electron laser," *Physical Review Special Topics-Accelerators and Beams*, vol. 12, no. 3, article 030702, 2009.

[35] P. R. Ribič, A. Abrami, L. Badano et al., "Coherent soft X-ray pulses from an echo-enabled harmonic generation free- electron laser," *Nature Photonics*, vol. 13, no. 8, article 427, pp. 555–561, 2019.

[36] C. Feng, H. Deng, M. Zhang et al., "Coherent extreme ultraviolet free-electron laser with echo-enabled harmonic generation," *Physical Review Accelerators and Beams*, vol. 22, no. 5, article 050703, 2019.

[37] C. J. Milne, T. Schietinger, M. Aiba et al., "SwissFEL: the Swiss X-ray free electron laser," *Applied Sciences*, vol. 7, no. 7, article app7070720, p. 720, 2017.

[38] S. Reiche, "GENESIS 1.3: a fully 3D time-dependent FEL simulation code," *Nuclear Instruments and Methods in Physics Research Section A: Accelerators, Spectrometers, Detectors and Associated Equipment*, vol. 429, no. 1-3, article S016890029900114X, pp. 243–248, 1999.